Journal of Catalysis 270 (2010) 95–102

Contents lists available at ScienceDirect

Journal of Catalysis

journal homepage: www.elsevier.com/locate/jcat

Selective adsorption of manganese onto cobalt for optimized Mn/Co/TiO_2 Fischer–Tropsch catalysts

Theresa E. Feltes [a], Leticia Espinosa-Alonso [b], Emiel de Smit [b], Lawrence D'Souza [a,1], Randall J. Meyer [a], Bert M. Weckhuysen [b], John R. Regalbuto [a,*]

[a] Department of Chemical Engineering, University of Illinois, MC 110 810 S Clinton Street, Chicago, IL 60607-7000, USA
[b] Inorganic Chemistry and Catalysis, Debye Institute for Nanomaterials Science, Utrecht University, Sorbonnelaan 16, 3584 CA Utrecht, The Netherlands

ARTICLE INFO

Article history:
Received 25 September 2009
Revised 8 December 2009
Accepted 12 December 2009
Available online 25 January 2010

Keywords:
Catalyst preparation
Cobalt
Manganese promotion
Fischer–Tropsch
Strong Electrostatic Adsorption

ABSTRACT

The Strong Electrostatic Adsorption (SEA) method was applied to the rational design of a promoted Co catalyst for Fischer–Tropsch (FT) synthesis. A series of Mn/Co/TiO_2 catalysts were prepared by selective deposition of the $[MnO_4]^-$ anion onto the supported Co_3O_4 phase. Qualitative ICP-OES and XPS measurements of the prepared catalysts with increasing Mn loading displayed the preferential association of the Mn species with Co_3O_4 and not the TiO_2 support. The SEA preparation method seemed to minimize the migration of Mn away from the Co to the TiO_2 support during reduction procedures to ensure a more intimate interaction between the Mn and the Co species during FT reactivity measurements. This led to an increase in light olefins, C_{5+} selectivity and chain growth probability. It is anticipated that the SEA preparation method is a viable synthesis strategy for other promoted and/or bimetallic catalyst systems where intimate contact between the catalyst components is highly desired.

1. Introduction

Promotion of heterogeneous catalysts is a ubiquitous, but poorly understood phenomenon. The key in producing an effective promoted metal catalyst lies in the intimate promoter–metal interaction, as catalyst promotion is a local effect. Current industrial methods of catalyst preparation, such as sequential impregnation, co-mulling or co-precipitation, are not capable of ensuring this close contact between promoter and metal.

Schwarz proposed that one could utilize the electrostatic interactions between a metal ion and a charged support to direct the adsorption of a metal ion over surfaces containing two oxide fractions [1–3]. The concept behind this technique has been refined by Regalbuto et al., coined as the Strong Electrostatic Adsorption (SEA) method, which has been successfully applied to prepare highly dispersed, monometallic catalysts on a wide variety of oxide and carbon supports [4–7]. The naturally occurring hydroxyl (–OH) groups on the surface of an oxide become protonated or deprotonated when the contacting solution pH is acidic or basic, respectively. These charged hydroxyl groups are then able to attract metal complex ions in solution of opposing charge. The density of the charged hydroxyl groups on the oxide surface depends on its Point of Zero Charge (PZC), i.e., the pH at which the surface is neutrally charged. Demonstrated as a function of surface potential in Fig. 1, metal oxides having a basic PZC will have a greater density of positively charged sites in an acidic medium and will readily adsorb an anionic complex and vice versa. This lays the groundwork to perform selective adsorption over mixed metal oxide supports and even after common calcination and reduction procedures are employed, strong interaction between the promoter and metal often still exists.

In the current work, we examine the potential of the SEA preparation method for the synthesis of improved Mn-promoted Co-based Fischer–Tropsch (FT) catalysts. Exploration toward new transportation fuel alternatives, driven by the construction of new FT plants by several major corporate players [8–10], has brought resurgence in the research to improve FT catalyst selectivity. Supported Co catalysts have been shown to be superior for the creation of long-chained hydrocarbons from syngas with minimal water-gas shift activity [11]. As a promoter, Mn, in relatively high Mn:Co ratios, has demonstrated an increase in the selectivity toward longer chained hydrocarbons, particularly light olefins, by suppression of methane formation when in close association with the supported and unsupported Co phase [12–16]. In a similar system as presented here, but with the addition of Mn to a Co/TiO_2 catalyst (7 wt.% Co) by dry impregnation, Morales et al. described additional promotion effects, electronic and structural, that Mn adds to the Co/TiO_2 FT system [16–20]. They observed a characteristic increase in C_{5+} selectivity and light olefin production when

* Corresponding author. Fax: +1 312 996 0808.
E-mail address: jrr@uic.edu (J.R. Regalbuto).
[1] Present address: Shell Technology India Pvt. Ltd., Bangalore, Karnataka 560 099, India.

0021-9517/$ - see front matter © 2010 Elsevier Inc. All rights reserved.
doi:10.1016/j.jcat.2009.12.012

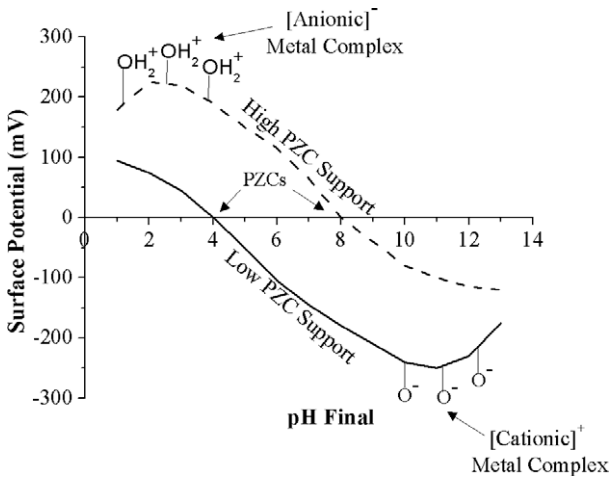

Fig. 1. Schematic of the selective adsorption of a metal complex by SEA, depicted as a function of surface potential.

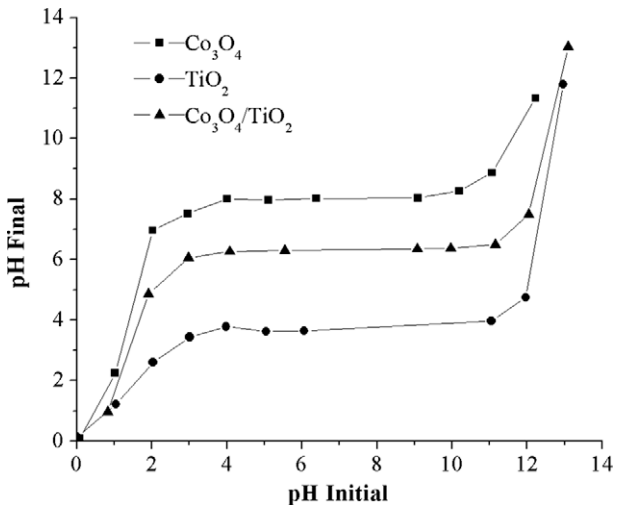

Fig. 2. PZC determination (indicated by the plateau [24]) of support materials at the high oxide surface loading of 10,000 m^2/L.

approaching a 3 wt.% MnO loading, but they also proposed that Mn increased turnover frequency (TOF), stabilized larger Co particles for an enhancement of activity and prevented negative effects caused by metal–support interactions [16,17]. However, they also noted migration of the Mn away from the Co to the TiO_2 support during reduction procedures minimizing promoter–metal contact [18,19]. Our SEA preparation method looks to minimize this phenomenon by creating an improved foundation to enhance Mn–Co interactions.

By utilizing an electrostatic driving force, this paper will describe the systematic preparation of a supported promoted metal catalyst, as the $[MnO_4]^-$ anion will be selectively adsorbed onto the Co_3O_4 (PZC = 8) fraction and not onto the TiO_2 (PZC = 3.7) support. The nature of the adsorption will be analyzed by UV–Vis spectroscopy and ICP-OES, while XPS, TPR, H_2 chemisorption and FT reactivity measurements will provide a well-rounded analysis on the effects of the catalyst preparation method used to enhance the interaction between Mn and Co in $Mn/Co/TiO_2$ FT catalysts.

2. Experimental

2.1. Adsorption experiments

Pure Co_3O_4 (BET surface area = 49 m^2/g) was prepared by the thermal decomposition of $Co(CO)_3{\cdot}xH_2O$ (Aldrich, 43–47%) at 350 °C for 24 h (5 °C/min ramp) [21]. The supported Co_3O_4 on TiO_2 (Aeroxide P25, BET surface area = 54 m^2/g) was performed via the homogeneous deposition precipitation [22] using $Co(NO_3)_2{\cdot}6H_2O$ (Merck, p.a.) as the precursor and urea (Acros, p.a.) as the precipitating agent as outlined by Morales et al. [16]. The filtered and washed solid was dried at room temperature overnight followed by calcination at 400 °C for 4 h (5 °C/min ramp). The formation of Co_3O_4 was confirmed with powder X-Ray diffraction (XRD) using a Bruker-AXS D8 diffractometer equipped with Co K_α radiation source (λ = 1.789 Å). The resulting material has a BET surface area of 58 m^2/g and a PZC of 6.3, which understandably lies between the PZCs of its bulk counterparts (Fig. 2).

Prior to the adsorption experiments, UV–Visible (UV–Vis) spectroscopy experiments were performed using a Varian Cary 50 spectrophotometer equipped with a Hellma immersion probe to monitor the behavior of $KMnO_4$ (Fluka, p.a.) in an acidic medium. The stability of the $[MnO_4]^-$ anion was of concern in the presence of HCl due to its known decomposition to tetra-, tri- and di-valent Mn compounds [23]. UV–Vis spectra of 200 mg/L Mn, as $KMnO_4$, solutions were recorded as a function of pH, ranging from 0.25 to neutral, after being shaken for 1 h. UV–Vis spectra on the stability as a function of time at pH 1, the predetermined optimal uptake pH of $[MnO_4]^-$ on Co_3O_4, were also analyzed.

Equilibrium adsorption experiments were performed at a surface loading, i.e., the total material surface area in solution, of 1000 m^2/L in excess liquid to prevent large shifts in the solution pH due to the oxide buffering effect [24]. The pH-adjusted solutions of $KMnO_4$ were contacted with Co_3O_4, TiO_2 and Co_3O_4/TiO_2 supports and shaken for 1 h, after which ~5 mL of filtered solution was analyzed for Mn concentration using a Perkin–Elmer Inductively Coupled Plasma-Optical Emission Spectrometer (ICP-OES). Mn uptake was determined as the difference in concentration between the pre- and post-contacted solutions. Additionally, ICP measurements for Co dissolution in the acidic medium were also performed, but proved negligible, concluding that the supported and unsupported Co oxides were stable.

2.2. Catalyst preparation and characterization

After determination of the optimal uptake pH, the supported Co_3O_4/TiO_2 material was loaded with increasing amounts of Mn as listed in Table 1 according to the adsorption experiments described above using various solutions with $KMnO_4$ as precursor. Weight loadings in Table 1 reflect the assumed final reduced states, Co^0 and MnO. After filtration of the solid, which were performed under the hood due to liberation of Cl_2 gas, the samples were dried at room temperature overnight and calcined at 350 °C for 4 h.

Powder XRD was again employed to evaluate Co_3O_4 morphology and crystallite size as a function of Mn loading (Table 1) via the line broadening analysis of the 70.5° and 77.8° 2θ reflections by application of the Scherrer equation.

X-ray Photoelectron Spectroscopy (XPS), used to analyze the surface of the calcined catalysts, was performed in a Kratos AXIS-165 Surface Analysis System. XPS analysis was carried out with a monochromatic Al X-ray source fitted with a charge neutralization coil. The binding energies (BE) were referenced to the C 1*s* peak at 285 eV. The survey and element scans for the O 1*s*, Ti 2*p*, Co 2*p* and Mn 2*p* core-level spectra were recorded.

Temperature Programmed Reduction (TPR) experiments were performed on a Micromeritics Autochem 2920 using a TCD detector. After stabilization of the baseline, the reduction was carried out at a heating rate of 10 °C/min in a 10% H_2/Ar flow.

Table 1
Compositions and properties of the FT catalysts studied.

Sample	Co (wt.%)	MnO (wt.%)	Co_3O_4 size[a] (nm)	XPS Co/Ti ratio	H_2 uptake (mmol/g)[b]
0.00MnCo	10.0	0.00	16.1	1.10	0.12
0.03MnCo	10.0	0.03	13.2	0.80	0.10
0.30MnCo	10.0	0.32	14.1	0.42	0.12
0.96MnCo	10.0	0.96	12.5	0.34	0.04
3.43MnCo	10.0	3.43	13.0	0.36	0.03

[a] Calculated from XRD results using Scherrer's equation.
[b] Based on H_2 chemisorption results.

H_2 chemisorption measurements were obtained using a Micromeritics ASAP 2020 following the method reported previously [14,16]. The samples were first dried at 120 °C in a He flow for 30 min and subsequently reduced in a 50% H_2/He flow at 350 °C for 2 h (ramp = 5°C/min). As suggested by Reuel and Bartholomew, the H_2 adsorption isotherms were measured at 150 °C, and calculations for the percentage Co dispersions were performed assuming a complete Co reduction with the stoichiometry of one hydrogen atom adsorbed per Co surface atom [25].

2.3. Catalyst testing

Fischer–Tropsch reactions of the Co/TiO_2 and Mn/Co/TiO_2 catalysts were investigated under isothermal plug-flow conditions achieved by diluting 50 mg of pre-sieved catalyst particles (0.2–0.5 mm) with 200 mg SiC (0.2 mm) in a glass reactor. Catalyst precursors were reduced prior to reaction for 2 h at 350 °C in H_2 at a heating rate of 5 °C/min. Reactions were performed at 1 bar, 220 °C and a syngas flow of 12 mL/min (H_2/CO = 2). Hydrocarbon products were analyzed using a Varian CP-3800 gas chromatograph equipped with a Flame Ionization Detector (FID). Catalytic performances were measured every 1 h for 20 h with selectivities compared at ~2% CO conversions.

3. Results and discussion

3.1. Permanganate stability and adsorption survey

UV–Vis measurements of the speciation of $KMnO_4$ in solution are shown in Fig. 3. The absorption bands of the $[MnO_4]^-$ anion contain a multiplet centered around 525 nm, a doublet around 320 nm and a shoulder around 240 nm. Fig. 3a represents the changes in the spectra as a function of increasing HCl concentration. As the pH becomes increasingly acidic, beyond a pH 2, distinct changes in the spectra are observed. At a pH of 1, there is the formation of two new absorption bands at 225 and 275 nm. Upon increasing acidity, the band at 225 nm diminishes and a new band at 250 nm forms. In addition, the 275 nm band disappears with the appearance of a shoulder around 340 nm. The spectrum is partially deteriorated at the extreme pH of 0.25 where solid MnO_2 was observed to form. We also see that the 250 and 340 nm features are still present, but the 225 and 275 nm contours disappear. This coincides with the analysis of the spectra as a function of time in Fig. 3b held at a pH of 1, the optimal uptake pH for Mn anion adsorption. The formation of the same absorption bands at 225 and 275 nm is seen in Fig. 3a, but they slowly diminish with increasing time indicating a transition from one species to another. The main observation is that the characteristic peaks for permanganate, around 525 nm, are effectively stable at the desired pH after 24 h, although, solutions were only held a maximum time of 15 min to before contacting it with the support.

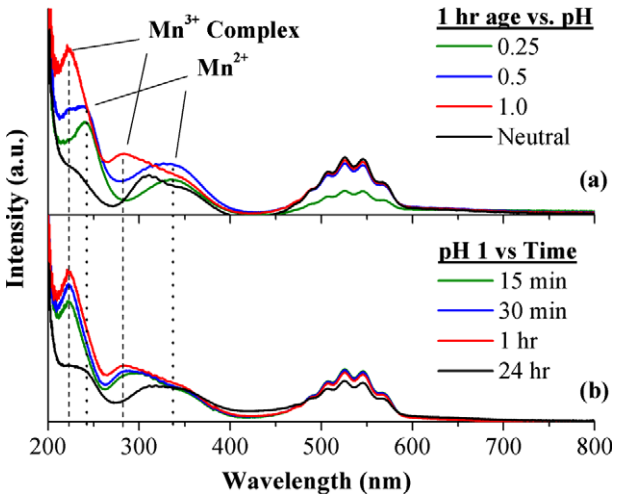

Fig. 3. UV–Vis spectra of $KMnO_4$ solution as a function of (a) pH and (b) time at pH 1.

$KMnO_4$ is known to speciate when placed in an acidic solution via the following pathways:

$$MnO_4^- + 8H^+ + 5Cl^- \rightarrow Mn^{2+} + 2.5Cl_2 + 4H_2O \quad (1)$$

$$MnO_4^- + 4H^+ + 3Cl^- \rightarrow MnO_2 + 2H_2O + 1.5Cl_2 \quad (2)$$

We already noted the presence of a brown solid forming in the solution at pH 0.25 as the formation of MnO_2 as justified in Eq. (2). The absorption bands at 225 and 275 nm have been reported as the presence of Mn^{3+} species [23,26] complexed either in the $[MnO_2]^-$ or $[MnCl_4]^-$ state. Thus, the appearance and disappearance of the bands at 225 and 275 nm as the pH changes from 1 to 0.5 implies a transition from a Mn^{3+} species to a Mn^{2+} species. The shoulder appearing at 340 nm has been previously attributed to molecular Cl_2 [27]. However, a $O_2^- \rightarrow Mn^{3+}$ charge transfer has also been used to explain this feature [28]. The complexes of the Mn^{3+} species that form should not affect the adsorption of Mn, since they are still in anionic state, but the presence of a Mn^{2+} cation at extreme pH will affect the adsorption concentration. The speciation of Mn as a function of pH with respect to the surface charge of the oxide support is illustrated in Fig. 4. The surface charge of the oxide was calculated based on the Revised Physical Adsorption (RPA) model [29,30]. It is clear that the Co_3O_4 contains a significantly higher density of positively charged sites than the TiO_2 in the range where anionic Mn species are present.

The permanganate adsorption results are shown in Fig. 5. The maximum uptake on TiO_2 was only 0.66 μmol/L Mn (0.16 wt.% Mn) when a possible 3.39 μmol/L Mn (0.99 wt.% Mn) was dissolved in solution (200 mg/L Mn). In comparison, Mn uptake on Co_3O_4 seems unbounded as it completely adsorbed 33.6 μmol/L Mn (9.09 wt.% Mn) of a 2000 mg/L Mn solution. Supported Co_3O_4 completely adsorbed 200 mg/L Mn solution, which is roughly the same Mn:Co ratio as the 2000 mg/L solution on pure Co_3O_4. The narrowness of the uptake volcano and its peak maximum differ from previous results seen with the adsorption of a Pt anionic complex with

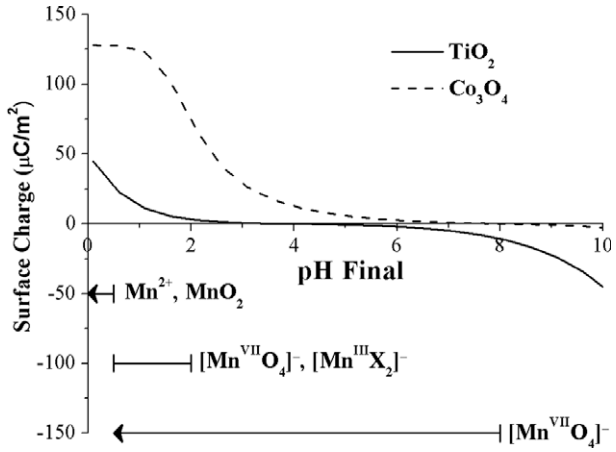

Fig. 4. Mn species present in solution as a function of pH with respect to oxide surface charge.

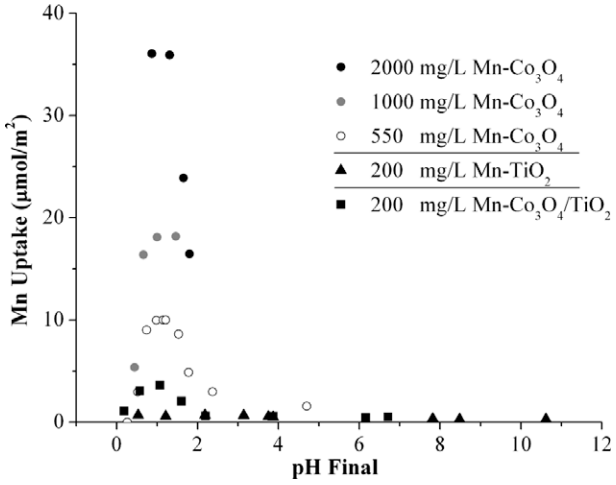

Fig. 5. $[MnO_4]^-$ pH vs. uptake survey over Co_3O_4, TiO_2 and supported Co_3O_4/TiO_2 at a surface loading of 1000 m^2/L.

SEA [31,32]. In the pH range from 1 to 3, the metal complex is in competition with the excess amount of Cl^- ions in solution for available adsorption sites due to increase of ionic strength at higher acid concentrations and, thus, a decrease in surface potential for complex adsorption. In this case, it is hypothesized that there is an additional step in the deposition mechanism beyond anion adsorption in which the Cl^- ions are actually enhancing the deposition of MnO_2 on the Co_3O_4 surface. The formation Mn^{2+} species below a pH of 1, as noted in the UV–Vis results, are actually contributing to the observed decrease in uptake.

As shown in Eqs. (1) and (2), the conversion of $[MnO_4]^-$ to MnO_2 requires both protons and chlorine anions, where, at a pH of 1, the surface of the Co_3O_4 is highly protonated and positively charged as noted by its surface charge in Fig. 4, attracting both Cl^- and $[MnO_4]^-$ ions to its surface. This reaction mechanism is also supported by the liberation of the product, Cl_2 gas, as mentioned previously, which only occurred in the presence of Co_3O_4. Additionally, XPS results indicated no residual Cl present on the catalyst surface, which, of course, is beneficial since Cl is known to be a poison to catalysts [33]. Thus, the mechanism of adsorption is also coupled with a reduction deposition step on the surface of the Co_3O_4, which is catalyzing the reaction to proceed. In addition, the natural redox properties that make Co_3O_4 useful in other partial oxidation surface reactions are also likely to enhance this reduction mechanism. The Co^{2+} and Co^{3+} oxidation states, which make up the Co_3O_4 structure, are known to easily transfer oxygen and readily interconvert under relatively mild conditions [34,35]. This permanganate reduction mechanism has also been reported to occur on carbon samples at 70 °C [36,37]. In addition, UV–Vis spectra, collected from the 200 ppm filtered solutions for all three supports at pH 1 (not shown here), agreed with ICP-OES results, supporting preferential $[MnO_4]^-$ adsorption at low pH when Co_3O_4 was present. The permanganate spectra remained stable after being in contact with the pure TiO_2 for 1 h, but completely vanished within 30 min of being in contact with the Co_3O_4 support materials. These unique adsorption measurements lead to the conclusion that Mn is being selectively adsorbed/deposited onto the Co_3O_4 surface and not the TiO_2 support. Based on these results, the optimal final pH of 1.0 was used to load various amounts of Mn onto the supported Co_3O_4 for further characterization experiments.

3.2. Characterization of prepared Mn-promoted Co-based FT catalysts

From XRD results, the calculated Co_3O_4 particle sizes by the Scherrer equation are given in Table 1. The particle size and morphology (Fig. 6) of the Co_3O_4 remained relatively constant after calcination as reflected in the peak broadening and positions. Any formation of mixed Co–Mn oxide spinels by the incorporation of Mn^{3+} into the Co_3O_4 lattice would be exhibited as a shift to lower 2θ values [17,38]. This indicates that Mn loading did not affect the structure of the bulk Co_3O_4. Therefore, although the Mn is in close association with Co, this method of preparation seems to limit the formation of $Co_{3-x}Mn_xO_4$ bulk solid solutions as seen previously with MnO loadings close to 3 wt.% [16].

To investigate the electronic state of Mn as well as its location with respect to the cobalt and titanium oxides, XPS spectra were collected for the catalysts after calcination. Fig. 7 displays the Co 2*p* XPS spectra as a function of Mn loading with the Co $2p_{3/2}$ and Co $2p_{1/2}$ binding energies at 780.1 eV and 795.1 eV, respectively, typical of Co_3O_4. As anticipated, Fig. 7 clearly displays a significant decrease in Co peak intensity with increasing Mn loading. However, if adsorption of permanganate was truly selective, the surface exposure of the Co should decrease relative to TiO_2 as the Mn loading is increased. Therefore, Co/Ti atomic ratios, as tabulated in Table 1, were collected from XPS spectra to determine extent of the Mn adsorption selectivity. The loading of the Mn on the samples resulted in a distinct lowering of the Co/Ti ratio from 1.10 to

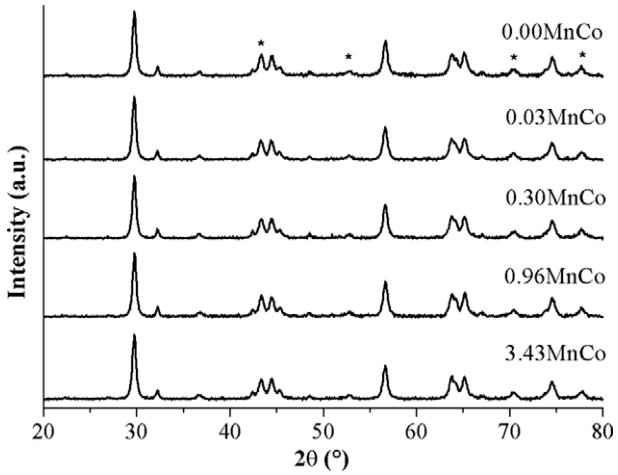

Fig. 6. XRD patterns of the unpromoted and promoted Co_3O_4/TiO_2 calcined materials with the strongest Co_3O_4 diffraction lines indicated by (∗).

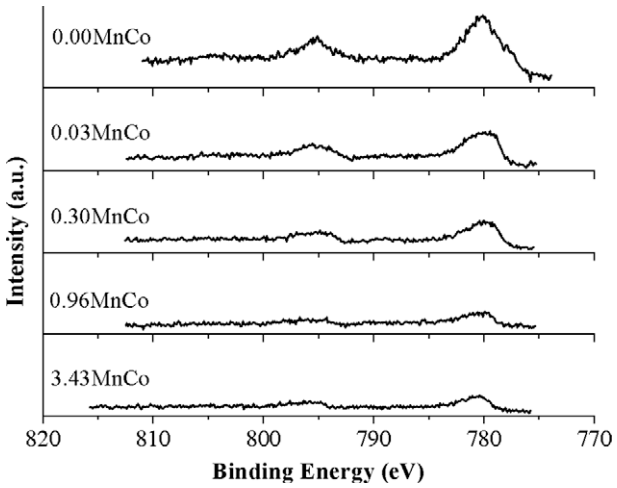

Fig. 7. Co 2*p* XPS spectra of calcined Co/TiO_2 and $Mn/Co/TiO_2$ catalysts.

0.36. This feature has been previously seen when Mn has been added as a promoter to a Co catalyst supported on a carbon nanofibers [14,39], where, the Mn was selectively partitioned on the Co due to the formation of a more energetically favorable stable state on the Co rather than the carbon support. Of course, migration of Mn could occur during the calcination step itself so the observation of the preferential association of Mn species with Co after calcination cannot be directly attributed to selective adsorption of permanganate. We see this possibility in the similar Co/Ti ratios for the 0.96–3.43 wt.% sample, where it seems that the 3.43MnCo has similar coverage than as the 0.96MnCo catalyst. This may be due to the possibility that the outer layer Mn species may not be as strongly bonded and thus we are seeing a migration to the TiO_2 surface caused by the calcination heat treatment.

With the addition of Mn to the catalyst, not only the intensity is affected, but also a slight broadening in the Co 2*p* shape is noted. As mentioned previously, characterization from XRD did not suggest the formation of Mn–Co spinel oxides, but this broadening may indicate the formation of some mixed oxide species on the surface of the Co particle. This has been reported to occur with Mn at low loadings [40], and it is evident that after calcination, there is formation to a small degree of some new Co species at the surface while the bulk Co_3O_4 remains stable.

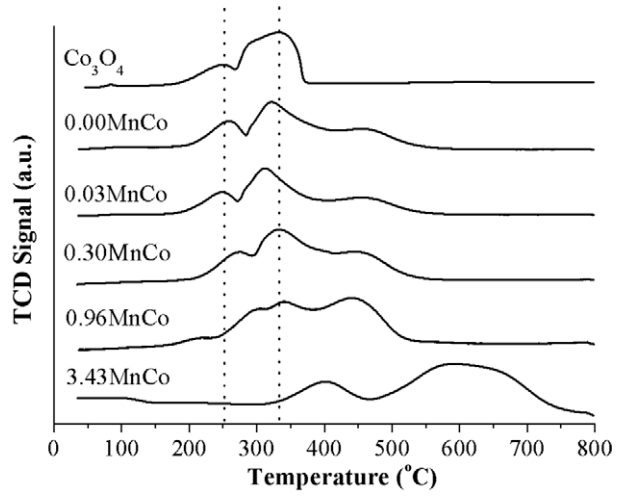

Fig. 8. TPR profiles of calcined catalysts. The dotted lines represent the stepwise reduction temperatures for bulk Co_3O_4.

When reduced, Co_3O_4 typically follows the two-step process: $Co_3O_4 \rightarrow CoO \rightarrow Co^0$. As seen from the TPR results in Fig. 8, these reduction steps normally occur at 250 °C and 330 °C in bulk Co_3O_4. Supporting the catalyst enhances the second step of the reduction to the Co^0 metal mainly due to the formation of smaller, dispersed particles. The additional peak in the supported catalyst at 460 °C has been reported as the partial reduction of TiO_2 induced by the presence of Co [41]. This can lead possible migration of TiO_x overlayers to block active Co sites. It has been speculated that Mn helps prevent the encapsulation of Co by reduced TiO_2 [16], but lower reduction temperatures prior to reactivity measurements are still employed to minimize this effect [42].

As Mn was added to the catalyst system, distinct changes occurred in the TPR profiles. It is known that Mn hampers the reduction of Co_3O_4 [14,16,43,44], but the effects of differences in the preparation procedure are seen to be significant. Interestingly, at the lowest loading of Mn, each stage of the Co reduction occurs 10 °C lower than the unpromoted sample. Therefore, it seems an enhancement of Co reducibility occurs with the addition of a small amount of Mn. As will be seen later, this is possibly related to the increase in activity in this sample by stabilizing the Co particles.

Previously, it has been reported that Mn mainly effects the Co^{2+} to Co^0 reduction [14,16], but due to the encasement of the Co_3O_4 by the Mn and the probable formation of Mn–Co spinels at the surface, as suggested from the XPS results, we are seeing a significant hindrance on both stages of the oxide reduction, especially in the highest Mn loading. This shows the specificity we can achieve in placement of the Mn over this catalyst.

The effects on the reducibility and coverage of Co_3O_4 are also reflected in the H_2 chemisorption measurements. H_2 chemisorption yields the number of Co^0 active sites available based on the uptake of H_2 as reported in Table 1. From the uptake results, the percentage dispersion and particle size of the Co^0 can be evaluated (Table 2). The adsorption measurements were performed after reduction at 350 °C for comparison to the reduction temperature used in FT reactivity measurements. As seen with the TPR results at this temperature, the degree of reduced Co varies. For the unpromoted sample, Morales et al. saw greater than 95% of the Co reduced at this temperature using a similar preparation procedure to support the Co [17]. From this and the TPR results, we can make the assumption that most of the Co is reduced after a 2-h reduction at 350 °C for the three lower Mn loadings and the 3.43MnCo is the only sample that has a lower percentage of reduced Co.

In Table 2, the particle size of Co^0 is estimated from the XRD data by ratioing the molecular masses of the Co and Co_3O_4. It is compared to the size estimated from the H_2 dispersion from the formula of Reuel and Bartholomew [25]. Particle size estimates for the Mn free sample are within reasonable agreement. As Mn loading increases, however, the XRD estimates remain largely the same while the H_2 chemisorption results decrease significantly. Since the TPR (Fig. 8) shows that all samples except the highest Mn loading should be fully reduced, the decrease in H_2 uptake is thought to be due to surface blockage. Beyond that, the 3.43MnCo sample is incompletely reduced (Fig. 8) and this will also cause a decrease in H_2 uptake.

Table 2
Comparison of estimated Co particle size based on XRD and H_2 chemisorption results.

Sample	XRD Est. Co size (nm)	H_2 Chemi. Co dispersion (%)	H_2 Chemi. Est. Co size (nm)
0.00MnCo	11.8	7.16	13.4
0.03MnCo	9.7	6.03	16.0
0.30MnCo	10.4	7.16	13.5
0.96MnCo	9.2	2.50	38.5
3.43MnCo	9.6	1.77	54.3

However, as seen in Table 1, some H_2 does adsorb on the 3.43MnCo catalyst, which signifies that a certain amount of Co is exposed and reduced. As mentioned above, XPS results lead us to believe some of the Mn is migrating off the surface of the Co during the calcination procedure thus leaving some of the Co oxide (or mixed Mn–Co oxide) exposed for reduction. Though we cannot deny that Mn migration occurs, which leads to a loss of selective interaction between the promoter and active metal, we can state there is a significant influence of the preparation method on the catalyst structure. Clearly, the Mn is initially in close association with the Co, and this method of preparation suggests a stronger degree of interaction after reduction procedures than previously published methods.

3.3. Fischer–Tropsch reactivity studies

The steady-state FT performance of the Mn-promoted Co/TiO_2 catalysts is compared in Table 3 and depicted in Fig. 9. The addition of small amounts of Mn (0.03MnCo) seems to slightly enhance the activity of the Co catalyst, but this feature disappears as loading is increased. The characteristic influence of a Mn species on enhancing C_{5+} selectivity is noted with an increase to 61 wt.% for the highest Mn loading. This is, of course, at the expense of the activity, which drops by 40%. Similar trends in activity and selectivities were seen when the Mn-promoted Co was supported on carbon nanofibers [14,39]. As mentioned previously, although catalysts prepared by dry impregnation should possess a more random distribution of both the active component and the promoter, the Mn stayed preferentially associated with the Co species due to an intrinsic thermodynamic driving force [14].

With regard to the TPR results, the reduction temperature of 350 °C contributes to different effects to the surface species with increasing Mn loading. We noted a slight improvement of reducibility of the Co upon addition of small amounts of Mn (0.03MnCo catalyst). When applied to FT synthesis, this catalyst displayed an enhanced activity. It has been speculated, when left unpromoted, Co can ripen and spread into smaller Co particles over the TiO_2 surface, which have shown to be less active [17]. This can be especially significant when on a TiO_2 support where migration of a reduced TiO_x phase onto smaller Co particles is facile. Thus, with the addition of a small amount of Mn, the Co^0 metal seems to be stabilized in a completely reduced state when compared to the unpromoted catalyst.

The opposite can be stated for the larger loadings of Mn. In this case, the preparation results in the placement of the Mn preferentially onto the Co_3O_4 contributing to the blockage active sites and hindered reducibility as described in the H_2 chemisorption discussion. The significance of these results is displayed in the olefin, C_{5+} selectivity and TOF rather than the activity. This increased selectivity is due to the higher ratio of Mn and Co interactions. This enhancement has been observed with supported and unsupported Co–Mn catalysts and is especially prominent at increased Co:Mn ratios [14–16,45–47]. Although there is a diminished activity, these catalysts have displayed superior time-on-stream stability

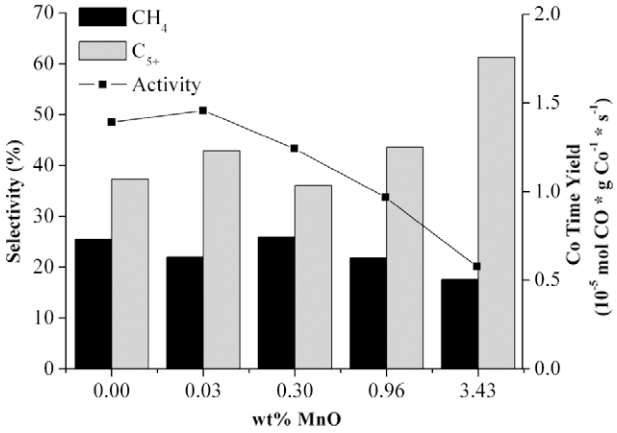

Fig. 9. Influence of manganese loading on selectivity and activity in the hydrogenation of CO at 220 °C and 1 bar.

at this reaction temperature [45]. There has not been much reported with regard to the Mn promotion effect on the TOF. Here, we are seeing higher TOFs for the higher Mn loaded catalysts. Morales et al. [17], also saw an increase in TOF with addition of Mn when compared to an unpromoted sample, but our findings are slightly contradictory to the results reported by Bezemer et al. [14] with respect to Mn loading, since these authors saw a decrease in TOF that has been related to the coverage of the Co^0 by MnO. It also must be mentioned that these results are calculated based on H_2 adsorption experiments and does not account for any changes in CO adsorption with respect to the state of Co or the presence of Mn. In fact, Jiang et al. have previously found that the presence

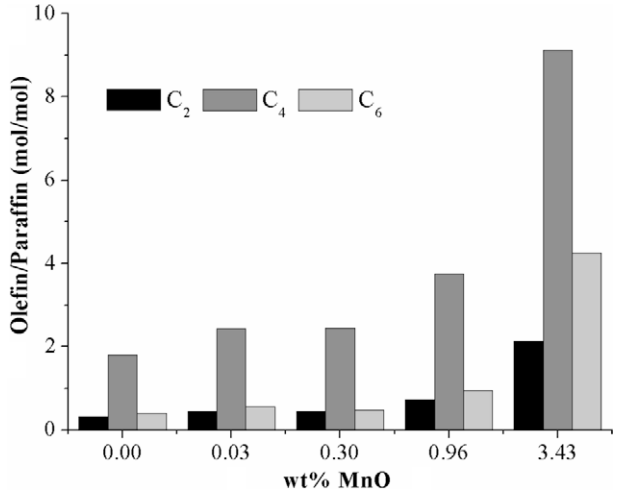

Fig. 10. Influence of manganese loading on the olefin to paraffin ratio for the C_2, C_4 and C_6 hydrocarbon products.

Table 3
FT catalytic performances of the Co/TiO_2 and $Mn/Co/TiO_2$ catalysts at 220 °C and 1 bar.

Sample	Activity[a]	TOF[b] (10^{-3} s^{-1})	CH_4 (wt.%)	C_{5+} (wt.%)	Chain growth probability (α)
0.00MnCo	1.39	11.5	25.5	37.4	0.62
0.03MnCo	1.46	14.3	22.0	43.0	0.64
0.30MnCo	1.24	10.2	26.0	36.1	0.61
0.96MnCo	0.97	22.8	21.9	43.6	0.65
3.43MnCo	0.58	21.7	17.6	61.3	0.81

[a] Activity: 10^{-5} mol CO g Co^{-1} s^{-1}.
[b] Calculated from H_2 chemisorption results.

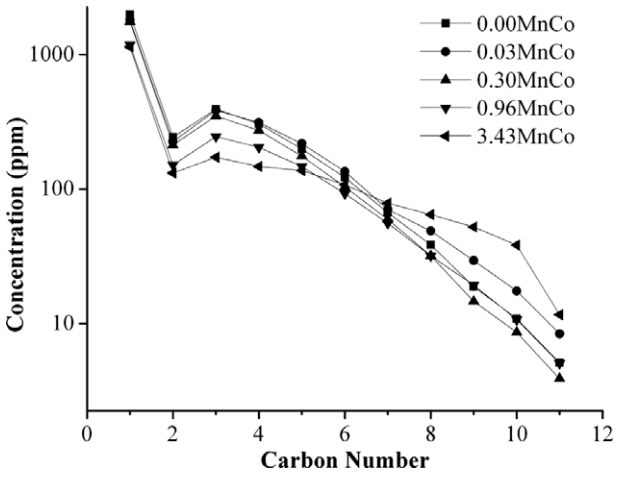

Fig. 11. ASF plot illustrating the influence of manganese on the chain growth probability and product distributions.

of Mn enhances CO adsorption [48] and therefore, our TOF values are based on an approximate number of active sites so caution must be taken in their interpretation.

Another significant effect on product selectivity is apparent in Fig. 10. As stated previously, Mn has been reported to enhance the industrially valued light olefin production by suppressing H_2 addition, the chain-growth terminating step [14–16]. Again, we are seeing clear demonstration of this in the C_2, C_4 and C_6 chains with increasing Mn loading, which are similar to trends previously reported [14,16]. For Fe–Mn catalysts, the high selectivity has been correlated by the presence of Fe–Mn spinel oxides [49]. Generally, it is reported that Mn be mainly present as MnO in its reduced state for FT catalysts [19,20,50], but it is apparent from the reduction temperature used that there will be some mixed oxide species present in the sample containing the highest Mn content. However, whether they are the Co_3O_4 spinel or some form of a Mn–Co spinel is inconclusive at this point.

Product distributions were calculated using the governing equation based on Anderson–Schulz–Flory (ASF) kinetics from the slope between C_3 and C_7 depicted in Fig. 11 [51,52]. This equation describes the product yield, which exponentially decreases with increasing chain length. Deviations, such as we see with the highest loadings of Mn, are described as a higher yield of longer hydrocarbons [11]. The cause of this deviation is due to the occurrence of a secondary reaction from the re-adsorption of α-olefin chains. Since re-adsorption reversed the termination, this is reflected in increase of the chain growth probability, α [11]. In conjunction with selectivity, the calculated values of the probability in Table 2 indicate the influence Mn has on chain growth and olefin production.

4. Conclusions

It is generally acknowledged that the efficient design of a promoted metal-based catalyst could effectively enhance the catalyst's performance. In this work, we have investigated the fundamental surface charging properties of an oxide in solution to achieve the selective adsorption of a Mn promoter onto the supported Co_3O_4 and not onto the TiO_2 support for Fischer–Tropsch synthesis. The current results indicate that the SEA preparation method allows us to quantitatively place the Mn promoter in close association with the Co with enhanced adsorption strength that is not achievable by dry impregnation. Thus, even with very small Mn additions, we presented a more active and stable Co catalyst, while at high Mn loadings, the catalyst selectivity is enhanced by a greater degree of Co and Mn interactions. This is achieved even when migration of the Mn promoter is known to take place during the reduction process, since the use of this preparation technique appears to limit it. Finally, we suggest that the use of SEA in the preparation of promoted catalysts is a viable strategy for the synthesis of any other promoted and/or bimetallic catalyst systems where intimate contact between the different catalyst components is highly desired.

Acknowledgments

T.E.F. gratefully acknowledges the help and support from the students and staff at Utrecht University; particularly Johan den Breejen for his assistance with the reactivity measurements. B.M.W. acknowledges NWO-CW and NCRSC-C for financial support. J.R.R. acknowledges the support of the National Science Foundation, CBET-0626505.

References

[1] J.A. Schwarz, Catal. Today 15 (1992) 395.
[2] J.A. Schwarz, C.T. Ugbor, R. Zhang, J. Catal. 138 (1992) 38.
[3] R. Zhang, J. Jagiello, J.F. Hu, Z.Q. Huang, J.A. Schwarz, A. Datye, Appl. Catal. A: Gen. 84 (1992) 123.
[4] J.R. Regalbuto, in: K.P. de Jong (Ed.), Synthesis of Solid Catalysts, John Wiley and Sons Ltd., Weinheim, 2009, p. 33.
[5] J.R. Regalbuto, in: R.M. Richards (Ed.), Surface and Nanomolecular Catalysis, Taylor & Francis/CRC Press, Boca Raton, 2006, p. 161.
[6] J.R. Regalbuto (Ed.), Catalyst Preparation: Science and Engineering, Taylor & Francis/CRC Press, Boca Raton, 2006, p. 297.
[7] L. D'souza, J.R. Regalbuto, J.T. Miller, J. Catal. 254 (2008) 157.
[8] M. Jacoby, Chem. Eng. News 86 (2008) 36.
[9] M.E. Dry, Catal. Today 71 (2002) 227.
[10] M.E. Dry, Appl. Catal. A: Gen. 276 (2004) 1.
[11] E. Iglesia, Appl. Catal. A: Gen. 161 (1997) 59.
[12] A.A. Mirzaei, M. Faizi, R. Habibpour, Appl. Catal. A: Gen. 306 (2006) 98.
[13] M. van der Riet, R.G. Copperthwaite, G.J. Hutchings, J. Chem. Soc., Faraday Trans. 1 83 (1987) 2963.
[14] G.L. Bezemer, P.B. Radstake, U. Falke, H. Oosterbeek, H.P.C.E. Kuipers, A. van Dillen, K.P. de Jong, J. Catal. 237 (2006) 152.
[15] M. van der Riet, G.J. Hutchings, R.G. Copperthwaite, J. Chem. Soc., Chem. Commun. 10 (1986) 798.
[16] F. Morales, E. de Smit, F.M.F. de Groot, T. Visser, B.M. Weckhuysen, J. Catal. 246 (2007) 91.
[17] F. Morales, D. Grandjean, A. Mens, F.M.F. de Groot, B.M. Weckhuysen, J. Phys. Chem. B 110 (2006) 8626.
[18] F. Morales, F.M.F. de Groot, O.L.J. Gijzeman, A. Mens, O. Stephan, B.M. Weckhuysen, J. Catal. 230 (2005) 301.
[19] F. Morales, D. Grandjean, F.M.F. de Groot, O. Stephan, B.M. Weckhuysen, Phys. Chem. Chem. Phys. 7 (2005) 568.
[20] F. Morales, F.M.F. de Groot, P. Glatzel, E. Kleimenov, H. Bluhm, M. Havecker, A. Knop-Gericke, B.M. Weckhuysen, J. Phys. Chem. B 108 (2004) 16201.
[21] G.A. El-Shobaky, A.S. Ahmad, A.L. Al-Noaimi, H.G. El-Shobaky, J. Therm. Anal. 46 (1996) 1801.
[22] J.W. Geus, Stud. Surf. Sci. Catal. 16 (1983) 1.
[23] A.V. Levanov, I.V. Kuskov, E.E. Antipenko, V.V. Lunin, Russ. J. Phys. Chem. A 80 (2006) 726.
[24] J. Park, J.R. Regalbuto, J. Colloid Interface Sci. 175 (1995) 239.
[25] R.C. Reuel, C.H. Bartholomew, J. Catal. 85 (1984) 63.
[26] D.G. Lee, C.R. Moylan, T. Hayashi, J.I. Brauman, J. Am. Chem. Soc. 109 (1987) 3003.
[27] D. Maric, J.P. Burrows, R. Meller, G.K. Moortgat, J. Photochem. Photobiol. A 70 (1993) 205.
[28] A.B.P. Lever, Inorganic Electronic Spectroscopy, Elsevier, Amsterdam, 1984.
[29] K.B. Agashe, J.R. Regalbuto, J. Colloid Interface Sci. 185 (1997) 174.
[30] X. Hao, W.A. Spieker, J.R. Regalbuto, J. Colloid Interface Sci. 267 (2003) 259.
[31] J.R. Regalbuto, A. Navada, S. Shadid, M.L. Bricker, Q. Chen, J. Catal. 184 (1999) 335.
[32] M. Schreier, J.R. Regalbuto, J. Catal. 225 (2004) 190.
[33] C.H. Bartholomew, Appl. Catal. A: Gen. 212 (2001) 17.
[34] S.C. Petitto, E.M. Marsh, G.A. Carson, M.A. Langell, J. Mol. Catal. A 281 (2008) 49.
[35] M. Longhi, L. Formaro, J. Electroanal. Chem. 464 (1999) 149.
[36] S.B. Ma, Y.H. Lee, K.Y. Ahn, C.M. Kim, K.H. Oh, K.B. Kim, J. Electrochem. Soc. 153 (2006) C27.
[37] S.B. Ma, K.Y. Ahn, E.S. Lee, K.H. Oh, K.B. Kim, Carbon 45 (2007) 375.
[38] E. Vila, R.M. Rojas, J.L.M. de Vidales, O. Garcia-Martinez, Chem. Mater. 8 (1996) 1078.

[39] G.L. Bezemer, U. Falke, A.J. van Dillen, K.P. de Jong, Chem. Commun. (2005) 731.
[40] H.J. Kim, M.K. Han, S.M. Lee, D.K. Hwang, Y.G. Shul, Top. Catal. 47 (2008) 109.
[41] Y. Shao, W. Chen, E. Wold, J. Paul, Langmuir 10 (1994) 178.
[42] R. Zennaro, M. Tagliabue, C.H. Bartholomew, Catal. Today 58 (2000) 309.
[43] A. Martinez, C. Lopez, F. Marquez, I. Diaz, J. Catal. 220 (2003) 486.
[44] D.H. Yin, W.H. Li, W.S. Yang, H.W. Xiang, Y.H. Sun, B. Zhong, S.Y. Peng, Microporous Mesoporous Mater. 47 (2001) 15.
[45] S. Colley, R.G. Copperthwaite, G.J. Hutchings, M. van der Riet, Ind. Eng. Chem. Res. 27 (1988) 1339.
[46] D. Das, G. Ravichandran, D.K. Chakrabarty, Appl. Catal. A: Gen. 131 (1995) 335.
[47] R.G. Copperthwaite, G.J. Hutchings, M. van der Riet, J. Woodhouse, Ind. Eng. Chem. Res. 26 (1987) 869.
[48] M. Jiang, N. Koizumi, T. Ozaki, M. Yamada, Appl. Catal. A: Gen. 209 (2001) 59.
[49] A.A. Mirzaei, R. Habibpour, E. Kashi, Appl. Catal. A: Gen. 296 (2005) 222.
[50] S.E. Colley, R.G. Copperthwaite, G.J. Hutchings, S.P. Terblanche, M.M. Thackeray, Nature 339 (1989) 129.
[51] R.B. Anderson, R.A. Friedel, H.H. Storch, J. Chem. Phys. 19 (1951) 313.
[52] P.J. Flory, Principles of Polymer Chemistry, Cornell Univ. Press, Ithaca, 1953.